Conductivity measurements in a shear-banding wormlike micellar system

Panos J. Photinos,[1] M. R. López-González,[2,*] Corey V. Hoven,[1,†] and Paul T. Callaghan[2]
[1]*Department of Physics, Southern Oregon University, Ashland, Oregon 97520, USA*
[2]*MacDiarmid Institute for Advanced Materials and Nanotechnology, Victoria University of Wellington, Wellington, New Zealand*
(Received 11 February 2010; published 9 July 2010)

Shear banding in the cetylpyridinium chloride/sodium salicylate micellar system is investigated using electrical conductivity measurements parallel to the velocity and parallel to the vorticity in a cylindrical Couette cell. The measurements show that the conductivity parallel to the velocity (vorticity) increases (decreases) monotonically with applied shear rate. The shear-induced anisotropy is over one order of magnitude lower than the anisotropy of the N_c nematic phase. The steady-state conductivity measurements indicate that the anisotropy of the shear induced low-viscosity (high shear rate) phase is not significantly larger than the anisotropy of the high viscosity (low shear rate) phase. We estimate that the micelles in the shear induced low viscosity band are relatively short, with a characteristic length to diameter ratio of 5–15. The relaxation behavior following the onset of shear is markedly different above and below the first critical value $\dot{\gamma}_1$, in agreement with results obtained by other methods. The transient measurements show that the overall anisotropy of the sample decreases as the steady state is approached, i.e., the micellar length/the degree of order decrease.

DOI: 10.1103/PhysRevE.82.011502 PACS number(s): 83.80.Qr, 83.60.Rs, 82.70.Uv, 83.80.Xz

I. INTRODUCTION

In recent years, an increasing number of micellar systems have been shown to exhibit shear banding [1]. In terms of rheological behavior, shear banding usually results into a flat shear stress plateau in the flow curve (shear stress σ, versus shear rate $\dot{\gamma}$) for shear rates between $\dot{\gamma}_1$ and $\dot{\gamma}_2$, the first and second critical values, respectively. Figure 1 is a schematic illustration of the main features of interest to the discussion that follows.

The stress plateau can be explained by assuming a double-valued flow curve [2–4]. For $\dot{\gamma}$ below the critical value $\dot{\gamma}_1$ the system follows the branch of low shear rate, and for $\dot{\gamma}$ above the second critical value $\dot{\gamma}_2$ the system follows the branch of high shear rate. For $\dot{\gamma}$ between $\dot{\gamma}_1$ and $\dot{\gamma}_2$ a fraction x of the system follows the branch of high shear rate, and a fraction $(1-x)$ follows the branch of low shear rate. As the shear stress in the plateau remains constant, we have $\sigma = \eta_1 \dot{\gamma}_1 = \eta_2 \dot{\gamma}_2$, where η_1 and η_2 are the corresponding viscosity values of the two branches at $\dot{\gamma}_1$ and $\dot{\gamma}_2$, respectively. Thus the plateau region reflects the coexistence of two phases of different viscosity. In a cylindrical Couette cell of gap d, one could visualize two layers: a high shear rate layer on the side of the rotating cylinder, of thickness $\sim xd$ with shear rate $\dot{\gamma}_2$; a low shear rate layer of thickness $\sim(1-x)d$ with shear rate $\dot{\gamma}_1$ and an interface/transition zone between the two layers. Therefore, at the plateau region of the flow curve, the shear rate is not constant across the gap of the flow cell. Consequently we speak of the "apparent shear rate" given by the lever rule,

$$\dot{\gamma} = x\dot{\gamma}_2 + (1-x)\dot{\gamma}_1. \quad (1)$$

The experimental results, including birefringence [5], particle image velocimetry (PIV) [6], light scattering [7], and NMR spectroscopy/imaging [8], establish the coexistence of bands with different shear rates.

Recent work shows that the shear banding is more complex than the simple two band model suggests. Significant insight, using various techniques, was gained by space-resolved and time-resolved measurements that probe the steady state and transient development of shear banding. The results demonstrate the existence of more than two bands [9–11], temporal and spatial undulations [12–15], formation of Taylor-like vortices [15,16], and different dynamics in the evolution of shear profile and the birefringence profile [17,18].

In terms of rheometric behavior, upon shear start-up in the plateau region, the shear stress shows a sharp overshoot [19]. The amplitude of the overshoot increases with increasing apparent shear rate, and can significantly exceed the steady state value of the shear stress. Following the overshoot, the shear stress may undergo one or more cycles of damped oscillation, lasting for several seconds before reaching the steady state value. In some cases, the shear stress may undershoot well below the steady state value [14,19]. At high shear rates, the fluctuations may persist indefinitely [12,13]. Birefringence, flow visualization and velocimetry studies [10,14,18,20] on systems similar to the one used in the present study show that the shear induced phase is initiated over the entire gap upon shear startup. This process corresponds to the stress overshoot, and occurs in a time scale of about 1 s, which is followed by the appearance of a diffuse interface that begins to migrate from the stationary cylinder. The interface sharpens as the migration slows down and finally stops. This process occurs within a few seconds and corresponds to the oscillatory transient. Following this process, and depending on the value of the apparent shear rate, the profile of the interface may show stable oscillating modes

*Present address: Department of Clinical Physics, Faculty of Medicine, University of Glasgow, Scotland, UK.
†Present address: Department of Materials, University of California, Santa Barbara, California 93106.

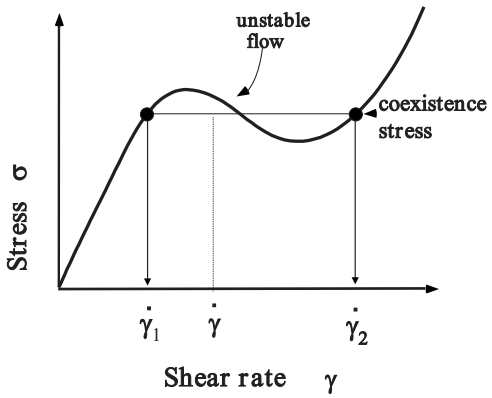

FIG. 1. Schematic illustration of flow curve of shear banding fluid.

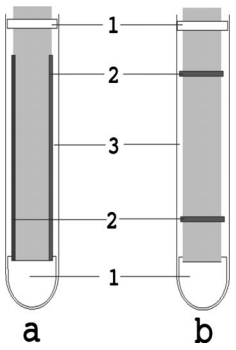

FIG. 2. Cell geometry (a) for $k_{\|}$ measurement and (b) for $k_{\perp}$ measurement. 1 Teflon spacers, 2 silver electrodes, 3 glass cell.

or chaotic behavior at higher shear rates. Lettinga and Manneville [20] showed that wall slippage may compete with or suppress shear banding and that for more entangled systems the high shear rate band may alternately nucleate-melt, which may account for the fluctuations observed in these systems at high shear rates [12,13]. Recent theoretical models support a three dimensional structure, including instabilities and chaotic response [21–25]. Recent reviews of experimental [26,27] and theoretical developments [28,29] detail the complexities and challenges presented in the study of shear banding fluids.

Of the micellar systems that are known to exhibit shear banding, the most studied are the hexadecyl-trimethyl-ammonium bromide (CTAB) system [30,31] and the cetylpyridinium chloride (CPyCl) system [32,33]. In this work we present measurements on the CPyCl system. In the range of concentrations of interest to the present study, the system shows a rather robust plateau at low shear rates with $\dot{\gamma}_1$ in the order of $1-10$ s^{-1}, and relaxation behavior below $\dot{\gamma}_1$ markedly different than in the plateau region [34,35]. It is interesting to note that the onset of the shear banding occurs at relatively low shear rates and for compositions that are far from the transition to a nematic phase. The nematic phase appears at surfactant concentrations ~35% (weight/volume) [34].

Conductivity measurements have been used to study shear thickening micellar systems [36,37], concentrated isotropic micellar solutions [38] and hexagonal micellar smectic phases [39]. The measurements provide insight on the symmetry and geometry of the micelles. The objective of the present work is to study the effect of shear induced stretching and alignment of the micelles on the conductivity of the micellar solution. The values of the conductivity and the conductivity anisotropy in particular, are sensitive to the shape and alignment of the micelles, and thus provide a probe of the alignment and shape of the micelles in the steady state, and the transient behavior. The conductivity results should be comparable [40] to the average intrinsic birefringence [41] of the sample. Unfortunately, the intrinsic birefringence cannot always be readily separated from the form birefringence, which for the most common micellar systems may have opposite sign than the intrinsic part [9] and from the shear induced dichroism [42]. The conductivity method has the additional advantage that it can be applied to opaque systems as well.

In what follows, we will assume that application of shear induces uniaxial symmetry, and denote the conductivity parallel to the symmetry axis by k_1, and the conductivity perpendicular to the symmetry axis by k_2. The anisotropy of the conductivity tensor is given by the difference k_1-k_2 which is analogous to the birefringence. The sign of k_1-k_2 can be positive or negative, depending on the shape of the micelles. For theoretical and numerical calculations, it is convenient to introduce the reduced anisotropy,

$$\alpha = (k_1 - k_2)/\langle k \rangle, \tag{2}$$

where the average value

$$\langle k \rangle = (k_1 + 2k_2)/3. \tag{3}$$

Dividing k_1-k_2 by the average value in the definition of α as given by Eq. (2) has the advantage of eliminating factors that affect the conductivity equally in all directions, e.g., ionic impurities. As we shall see below, and as long as the temperature is constant, the variation of $\langle k \rangle$ is very weak, therefore k_1-k_2 and α differ by an essentially constant factor.

From Eq. (3) above, it follows immediately that

$$k_1 - \langle k \rangle = 2(\langle k \rangle - k_2). \tag{4}$$

Therefore, as long as the average value $\langle k \rangle$ remains the same, an increase in k_1 due to, for example, a change in the degree of alignment of the micelles, will be twice as large as the change in k_2 and of the opposite sign.

The conductivity for arbitrary directions at an angle χ to the principal symmetry axis of the phase is related to k_1 and k_2 by

$$k(\chi) = k_1 \cos^2 \chi + k_2 \sin^2 \chi. \tag{5}$$

Measurements in aligned micellar phases [39,40,43,44] and numerical calculations [45,46] show that, for given concentration, the reduced anisotropy α depends on the degree of alignment of the micelles and the geometry of the micelle. The degree of alignment is measured by the order parameter

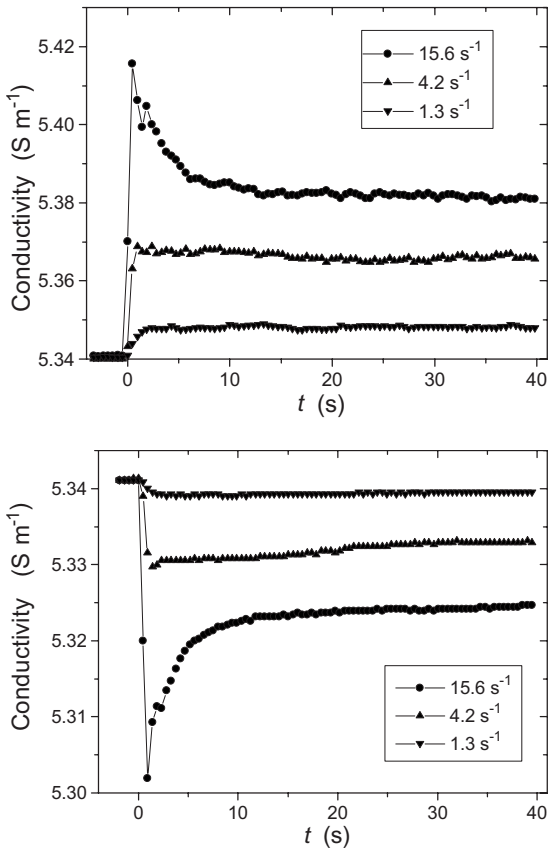

FIG. 3. (a) Typical results for conductivity measurements parallel to the velocity, at three different shear rates: (▼) 1.3 s^{-1} ; (▲) 4.2 s^{-1} and (●)15.6 s^{-1}. Line segments added as guide to the eyes. (b) Typical results for conductivity measurements parallel to the velocity, at three different shear rates: (▼) 1.3 s^{-1} ; (▲) 4.2 s^{-1}, and (●)15.6 s^{-1}. Line segments added as guide to the eyes.

$$S = \frac{1}{2}\langle 3\cos^2\theta - 1\rangle, \tag{6}$$

where the brackets indicate average value over the entire sample, and θ is the angle between the axis of the micelle and the symmetry axis of the phase. The value of S can be measured by small angle neutron scattering [47] and is in the order of 0.6. The anisotropy at a given degree of order is:

$$\alpha = \alpha_o S, \tag{7}$$

where α_o is the anisotropy at perfect alignment. The value of α_o depends only on the shape, the spatial arrangement and the volume fraction occupied by the micelles.

Experimental and theoretical results show that for the elongated micelles of the so-called N_c nematic phase, the reduced anisotropy α is positive [40,44], and increases with micellar length (the diameter of the micelle is essentially constant, approximately equal to twice the length of the surfactant molecule) and with degree of alignment of the micelles. The calculations also show that for given ionic concentration and ionic mobility, the average value tends to decrease as the micelles get longer [45,46]. Comparison of the theoretical calculations and the measured anisotropies allows estimates of the length to diameter ratio of the micelles. Typical values are in the range of 3–15 for the N_c phase [40,44].

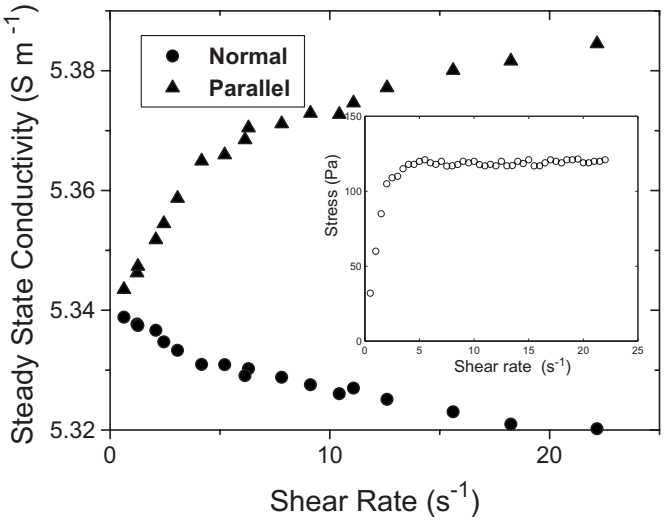

FIG. 4. (▲) Steady state conductivity parallel to the velocity $k_{\|}$ for various shear rates.(●)Steady state conductivity parallel to the vorticity (normal to the velocity) $k_{\perp}$ for various shear rates. For both components, a change in the slope occurs at about $\dot{\gamma}$=4 s^{-1}. The inset shows the flow curve data for this system adapted from Ref. [13].

In what follows, we will present conductivity measurements parallel to the velocity and parallel to the vorticity. Steady state values for both geometries will be presented as a function of $\dot{\gamma}$. We will also present time resolved measurements showing the transient behavior on shear start-up. The results will be used to discuss the length and alignment of the micelles in the steady state and in the transient response.

II. EXPERIMENTAL

A. Sample preparation

The samples used in our measurements were prepared by mixing CPyCl (from Sigma) and sodium salicylate, NaSal (from Fluka) at molar ratio 2:1. The materials (min purity >99%) were used as received. The mix of dry CPyCl and NaSal was dissolved in 0.5 M H_2O NaCl brine. For the measurements reported here we use a 10% (weight/volume) of (CPyCl+NaSal) in 2:1 molar ratio. The samples were allowed to equilibrate at 30 °C for several days before using.

B. Rheological properties

Rheological measurements for the sample composition used in the present measurements [12,13] show linear behavior up to about $\dot{\gamma}$=1.2 s^{-1}, shear thinning between $\dot{\gamma}$=1.2 to 2.8 s^{-1}, followed by a plateau that extends from $\dot{\gamma}_1$ =2.8 s^{-1} to at least 40 s^{-1}. The elastic plateau modulus G_0 =256 Pa, the Maxwell relaxation time τ=0.46 s, and the mesh size ξ=11 nm. In shear start-up measurements [13] when the apparent shear rate is $\dot{\gamma} > \dot{\gamma}_1$ the shear stress shows noticeable overshoot for about 1 s. The relaxation following

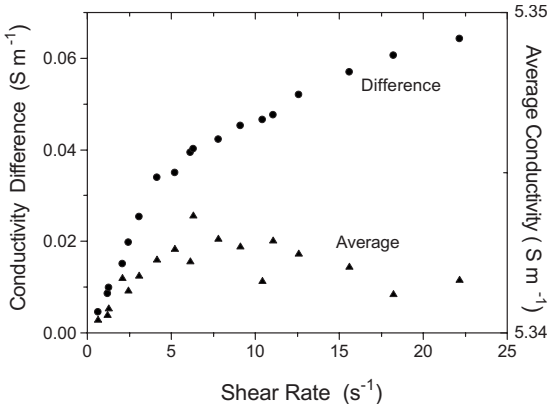

FIG. 5. (●) difference between the two measured conductivities, $k_{\|}-k_{\perp}$ for various shear rates. (▲) Average value, calculated as $(k_{\|}+2k_{\perp})/3$. Values are slightly, but consistently above the value of the conductivity at zero shear.

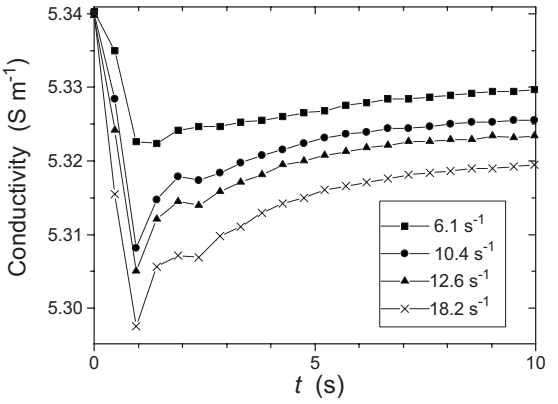

FIG. 6. Time resolved conductivity $k_{\perp}$ for four start-up experiments. Sample was initially at rest. Shear was applied at t=0, at shear rate of: (■) $\dot{\gamma}=6.1$ s^{-1} ; (●) $\dot{\gamma}=10.4$ s^{-1}; (▲) $\dot{\gamma}=12.6$ s^{-1}; and (×) $\dot{\gamma}=18.2$ s^{-1}. Line segments added as guide to the eyes.

shear start-up depends on the applied shear rate, and shows persistent fluctuations for high shear rates. For example, at shear rate $\dot{\gamma}=30$ s^{-1} an oscillatory behavior persists for over 1000 s. It is worth noting nevertheless, that different batches of material are known to give different dynamics [12].

C. Conductivity cells

We designed two conductivity cells to measure the resistance parallel to the velocity and parallel to the vorticity (i.e., parallel to the long axis of the cylindrical cell). The geometry of the cells is shown schematically in Fig. 2. The cells were constructed using precision glass tubes (Wilmad Laboratory Glass, inner diameter 20 mm) as the outer (rotating) cylinders. The inner (stationary) cylinders (diameter 18 mm) were machined from Plexiglas rod. The outer glass cylinder allows visual observation of the sample, which is particularly helpful during the filling process. The cylinder spacers were machined from Teflon. Silver electrodes were painted (Flexible Silver 13, Engelhard, N.J.) on the inner cylinder. To measure the conductivity parallel to the velocity, the electrodes (about 5 cm long, 1mm wide, 10 μ thick) were deposited on the surface of the inner cylinder, diametrically opposite and parallel to the axis of the cylinder. For conductivity parallel to the vorticity, we deposited two parallel rings on the inner cylinder, spaced 5 cm apart. The outer cylinder of the cell was fit into a machined Teflon holder that was driven by a computer controlled step motor.

D. Conductivity measurements

The resistance was measured using a LCR meter (Stanford Research Systems, Model SR720, accuracy 0.05%, precision 0.001%). All the measurements were carried out at 1 kHz frequency, and the signal amplitude was 0.1 V. The LCR was configured in the parallel circuit, $R+Q$ mode, and the value of Q (ratio of imaginary to real impedance) was negative and less than 3%. The frequency dependence of the measurements in the 1 to 10 kHz range was less than 0.6%, which together with the low Q value indicate that the impedance of the sample was essentially Ohmic, with a small capacitive contribution, and that electrode polarization effects are minimal. The conductivity cells were calibrated using a 0.5 M KCl solution. The cell constants as derived from the calibration measurements were compared to the values calculated for a rectangular cell with two parallel electrodes, with dimensions corresponding to the dimensions of each of the conductance cells of Fig. 2. The agreement between measured and calculated values was better than 5% for the measurement parallel to the velocity and better than 2% for the normal direction. The agreement indicates that the edge effects produced by depositing the electrodes on the cylinder are small, and that the measurements essentially sample the entire gap. The conductivity values were derived from the resistance measurements by calibrating our cells against a standard conductivity cell (Topac, model SK23T). At 26 °C, the conductivity of the sample at zero shear rate was $k_0=5.3\pm0.1$ S m^{-1}. The uncertainty in k_0 is estimated from the purity of the chemicals used to prepare the samples.

The measurements were taken at time intervals of 0.47 s. In a separate measurement we determined that in the range of 25–60 °C, the conductivity of the CPyCl/NaSal micellar system used in the present experiments increases by about 1% per degree, which eventually proved to be of the same order of magnitude as the measured effect of shear. Therefore, it was necessary to thermally insulate the cell, especially from heat generated by the driving step motor, to minimize thermal drift. The measurements reported here were carried out at 26 °C. Unless indicated otherwise, the measurements were taken in a start-up mode, i.e., the sample was initially at rest for a period of 5 min, and the pre-selected shear rate was applied at $t=0$. In our measurements, the applied shear rate did not exceed 22 s^{-1}, due to the fact that at higher shear rates air bubbles appeared. Therefore, it was not possible to access the chaotic regime [12,13]. Following shear cessation, both $k_{\|}$ and $k_{\perp}$ recover in about 1–2 s, therefore, with the resolution of the present measurements it is not possible to detect the fine relaxation structure seen in the NMR spectroscopy measurements of the same micellar system [13].

From the geometry of the measurement it follows that on average, the major symmetry axis of the conductivity tensor

is in the shear plane, therefore, the measured $k_\perp$ is normal to the major symmetry axis, and corresponds to k_2. The major axis is not parallel to the velocity, therefore the measured $k_\parallel$ is not equal to k_1, and is given by Eq. (5). At zero shear rate, $\chi=45°$ which corresponds to a random orientation of the micelles. As the shear rate increases, χ decreases. For micelles completely aligned in the flow direction, $\chi=0°$. In the plateau region, optical measurements in the CPyCl system [9] and in the CTAB system [31] in the low shear rate band give an angle χ of about 20°. Point-wise birefringence measurements give $\chi\sim 0°$ near the rotating wall [18]. The measurements show that the difference between $k_\parallel$ and k_1 is small. It can be verified, using $k_\parallel$ and $k_\perp$ $(=k_2)$ values from Fig. 5 and $\chi=20°$ in Eq. (5), that the difference between $k_\parallel$ and k_1 is less than 0.9%. Therefore, the error resulting from using $k_\parallel$ instead of k_1 in the conductivity anisotropy or the average conductivity, is small.

III. RESULTS AND DISCUSSION

We carried out a series of measurements taken at 18 different shear flow rates, in the range of 0.5–22 s^{-1}. Representative results for three such measurements (for $\dot{\gamma}=1.3$, 4.2, and 15.6 s^{-1}) are shown in Fig. 3(a) for conductivity measurements parallel to the velocity, $k_\parallel$, and in Fig. 3(b) for conductivity measurements parallel to the vorticity, $k_\perp$, respectively. We note that for all values of applied shear rate the conductivity parallel to the velocity (vorticity) increases (decreases) compared to the conductivity at zero shear k_0. Thus, the applied shear induces anisotropy in the conductivity for all values of $\dot{\gamma}$. We also note that after an initial transient behavior, which depends strongly on the value of $\dot{\gamma}$, and will be discussed in more detail later in this section, the conductivity appears to settle to a steady-state value within the 40 s time interval shown in Figs. 3(a) and 3(b). In addition, the results clearly show that within the resolution of the experimental measurements, the features of $k_\parallel$ and $k_\perp$ mirror each other to considerable detail.

A. Steady state results

Figure 4 shows the steady state values of the conductivities in the two directions of the measurement for shear rate values in the range $\dot{\gamma}=0.5-22$ s^{-1}. The measurements show that the component parallel to the velocity (vorticity) increases (decreases) monotonically with increasing shear rate, i.e., no saturation is observed. Both components show a change in slope around $\dot{\gamma}=4$ s^{-1}. The change in the slope presumably corresponds to the onset of the stress plateau as determined from the flow curves for this system [34,35]. Therefore we set $\dot{\gamma}_1=4$ s^{-1}, which is in good agreement with values reported by López-González *et al.* [13] whose flow curve is shown (inset) in Fig. 4.

Comparing the conductivity along the two directions to the conductivity at rest, it is seen from Fig. 4 that for all values of $\dot{\gamma}$ the change in the conductivity parallel to the velocity is about twice the change in the conductivity in the normal direction and of the opposite sign. This result is in good agreement with Eq. (4) above. It must be remembered however that Eq. (4) applies to the principal values of the conductivity tensor, and assuming that the average value $\langle k\rangle$ remains constant (see discussion of Fig. 5 below).

The average quantity $(k_\parallel+2k_\perp)/3$ and the difference between the two conductivity values, $k_\parallel-k_\perp$, for the range of shear rate values investigated are shown in Fig. 5. As expected, the difference $k_\parallel-k_\perp$ shows a change in slope at about $\dot{\gamma}=4$ s^{-1}. The data in Fig. 5 show that for all shear rates, the sample is anisotropic, and that the anisotropy is positive, $k_\parallel-k_\perp>0$, i.e., has the same sign as the N_c micellar nematic phase. Below $\dot{\gamma}_1$ the sample is in a single phase, and the measured positive anisotropy can be understood in terms of the stretching of the micellar network which results in micellar segments oriented along the direction of flow. The length/degree of alignment of the stretched micellar segments increases as the applied shear rate is increased, leading to an increase (decrease) in $k_\parallel$ $(k_\perp)$, respectively. Above $\dot{\gamma}_1$ the high shear rate band appears, which presumably has a different value of anisotropy. Point-wise birefringence measurements [18] show that in the plateau region:

(i) the birefringence increases as we move from the stationary to the rotating wall;

(ii) for a given point in the gap (in high *or* low shear rate band) the birefringence increases as the apparent shear rate is increased;

(iii) the rate of increase in the birefringence as $\dot{\gamma}$ is increased, is comparable in the high and low shear rate bands, before the birefringence eventually reaches saturation in the high shear rate band;

(iv) the saturation value in the high shear rate band is about 1.5 times the birefringence of the low shear rate band.

In terms of conductivity, the point-wise birefringence measurements would suggest that:

(i) the conductivity anisotropy of the high shear rate band is larger than the anisotropy of the low shear rate band;

(ii) the anisotropy of *both* the low shear rate band and the high shear rate band will increase as the apparent shear rate is increased;

(iii) the rate of increase in the conductivity anisotropy as $\dot{\gamma}$ is increased, is comparable in the high and low shear rate bands;

(iv) for the range of apparent shear rates used in the present work, the conductivity anisotropy of the high shear rate band cannot be significantly larger than the anisotropy of the low shear rate band.

We can use the results of the point-wise birefringence measurement as a guide for the interpretation of our sample averaged conductivity measurements. The anisotropy of the sample is a combination of the anisotropy in the high and low shear rate bands. The data in Fig. 5, show that the conductivity anisotropy continues to increase as $\dot{\gamma}$ increases above $\dot{\gamma}_1$, but the slope with respect to $\dot{\gamma}$ is smaller than the slope below $\dot{\gamma}_1$ where the low shear rate band fills the entire gap of the cell. Therefore, the results of Fig. 5 are in agreement with the lever rule of Eq. (1) [7]. In addition, the results of Fig. 5 are consistent with the conclusion that the anisotropy in the high shear rate band is not significantly larger than the anisotropy in the low shear rate band. It is important to note that the conductivity anisotropy in the low shear rate band arises from stretched/aligned sections of entangled mi-

celles. Due to entanglement, a significant portion of the micelle length would be curved, and pointing in all directions, and thus not contributing to the conductivity anisotropy. In the high shear rate band the entanglement of the micelles is considerably reduced, and according to NMR measurements they have high degree of orientational order [12,13]. As the conductivity anisotropy does not increase drastically from the high to low shear rate bands, we conclude that the characteristic length over which the alignment of neighboring micelles persists in the high shear rate band is about the same or lower than the length of the stretched sections (persistence length) of the micelles in the low shear rate band. Assuming that the apparent persistence length in the low shear rate band grows to about two to five times the mesh size $\xi = 11$ nm (see experimental Sec. II B above) and the micellar diameter is about 4 nm, we estimate a characteristic length/diameter ($=L/D$) in the range of 5–15. This range of values is reasonable agreement with the estimates for the N_c phase listed in the introduction, although the latter refer to higher concentrations. The Onsager [48] model for hard rods predicts $L/D=45$ at the sample concentration used in this work. Therefore the length/diameter ratio in the shear induced phase is considerable lower than what one would theoretically expect for an equilibrium hard-rod N_c phase.

Measurements in aligned micellar liquid crystalline phases show that positive conductivity anisotropy obtains in aligned N_c (calamitic) nematic phases [40]. Conductivity measurements can be used to estimate the size of the micelles. Nesrullajev *et al.* [39] used conductance measurements in the hexagonal smectic phase to determine the rotational diffusion after shear cessation, and thus determine the length of the micelles. In the present work we compare the measured anisotropy to numerical calculations and estimate the micellar length. From the results of Figs. 4 and 5, it is clear that the shear induced anisotropy follows the symmetry of the N_c (calamitic) nematic phases. From the data of Fig. 5, the reduced anisotropy at the highest shear rate is

$$\alpha = 0.012.$$

In the more concentrated (about 35% by weight) solution of tetradecyltrimethyl ammonium bromide (MTAB) in D_2O, which shows an N_c nematic phase at room temperature, the measured anisotropy is $\alpha=0.12$, i.e., one order of magnitude higher [40].

Conductivity measurements in micellar systems under shear were presented by Gotz and Heckmann [38] on the CTAB system (19% by weight). They applied comparatively high shear-rates (in the range from 200 to 2500 s^{-1}) and did not report on the transient behavior. It is interesting to note that the reported anisotropy is of the same sign as measured in the present work, and that for temperatures <30 °C, the anisotropy saturates at the high-end of the shear rate. The anisotropy at saturation is about $\alpha \sim 0.15-0.20$, i.e., one order of magnitude larger than the values measured here for about half the concentration and much lower shear rates. The relatively low anisotropy values could reflect wall slippage [20]. They could also result from the appearance of negative anisotropy at high shear rates, for example, if the micelles in part of the gap were aligned parallel to the vorticity. On the basis of the conductivity results of Fig. 3, this appears unlikely, because the slope of $k_{\|}$ is about twice that of $k_{\perp}$ for all shear rates, as required by Eq. (4). Other factors that would affect the overall anisotropy of the sample could arise from the undulation of the interface profile across the vorticity direction, and the development of instabilities, as demonstrated experimentally by Lerouge *et al.* [14]. Numerical calculations would be necessary for a quantitative comparison.

As noted in the experimental section, the average quantity $(k_{\|}+2k_{\perp})/3$ is a good approximation to the average conductivity $\langle k \rangle$ of Eq. (3). From Fig. 5, we note that the average is slightly ($<0.1\%$ at maximum) but consistently larger than the value of the conductivity at zero shear rate. As discussed in the introduction, for given micellar concentration, the average value $\langle k \rangle$ increases with decreasing micellar length. Therefore, the (slight) increase in $\langle k \rangle$ is consistent with a decrease in micellar length.

B. Transient measurements

Transient behavior was reported in the original work of Rehage and Hoffmann [32]. The viscosity curves of Rehage and Hoffman are quite similar to the conductivity shown in Fig. 3(a). The transient behavior following shear start-up depends on the value of $\dot{\gamma}$, as demonstrated by various methods, for example in the work of Berret *et al.* [19,34] Hu and Lips [10]Holmes *et al.* [49] and López-González *et al.* [13]Miller and Rothstein [18] and Radulescu *et al.* [50].

Referring back to Figs. 3(a) and 3(b) we note a rather similar behavior in the two geometries of the conductivity measurements. Specifically, for the $\dot{\gamma}=15.6$ s^{-1} measurement (well above $\dot{\gamma}_1$) there is a marked overshoot (undershoot) of $k_{\|}$ ($k_{\perp}$) followed by a longer relaxation. For $\dot{\gamma}=4.2$ s^{-1} (near the lower end of the plateau) the initial overshoot/undershoot are hardly noticeable, while the longer relaxation is still discernible. The $\dot{\gamma}=1.3$ s^{-1} ($<\dot{\gamma}_1$) data in the resolution allowed by the present measurement, do not show overshoot, and the steady state is reached in about 1 s. This result is consistent with linear viscoelastic measurements at shear rates below $\dot{\gamma}_1$, that show relaxation times of the order of 0.5 s [13,34].

Figures 3(a) and 3(b) also show that the relaxation is captured in the behavior of both $k_{\|}$ and $k_{\perp}$, and that the time resolved variation of the two components occur in opposite direction, i.e., an overshoot in $k_{\|}$ corresponds to an undershoot in $k_{\perp}$. Therefore, we conclude that the entire relaxation process involves realignment of the micelles and/or changes in the size of the micelles. Also, as the values of $k_{\|}$ ($k_{\perp}$) during the transient behavior remain higher (lower) than the steady state value, we infer that during the relaxation processes, the overall alignment/length of the micelles is larger than in the steady state. In other words, the sample is more anisotropic while approaching the steady state.

Figure 6 shows the early part of the transient behavior for $k_{\perp}$ at four values of the apparent shear rate in the plateau. The figure reproduces the main features observed in the rheological and birefringence curves [9,13,19,34]. The initial sharp peak (negative, as expected for $k_{\perp}$) corresponds to the overshoot in the rheological/birefringence data, with a rise

time in the order of ~1 s, and amplitude increasing with increasing apparent shear rate. With reference to the stationary value of the conductivity the amplitude of the peak represents a change in conductivity that is comparable to the change induced at steady state. In terms of conductivity this variation translates into higher degree of order/longer micellar sections. Following the initial peak we observe a modest "overshoot" (for about ~1–3 s) which corresponds to the undershoot in the rheological/birefringence data, and a slow approach to the steady state value. Again, we note that $k_{\perp}$ remains well below the steady state value throughout the approach to steady state. We do not observe any variations of significant amplitude beyond the initial peak. It should be noted that the initial peak in rheometric curves can be one order of magnitude higher than the steady state stress [19]. In the birefringence [9,18] and the conductance measurements presented here, the initial overshoot is only a factor of 2 larger than shear induced increment in the steady state. Therefore, the oscillatory behavior [19] may be beyond the resolution of the conductance measurements. The final relaxation stage observed is the slow approach to the steady state. For the 15.6 s^{-1} measurements in Figs. 3(a) and 3(b), the fitted relaxation time is 4.3 ± 0.5 s. In terms of the interpretation of Lerouge *et al.* [14,15] the last stage reflects the destabilization of the interface, leading to waves, undulations, and vortices at higher shear rates. The transient behavior could also be interpreted in terms of wall slippage [20].

Radulescu *et al.* [50] proposed that the slow relaxation may reflect micellar migration from the low to the high shear rate band. The time scales derived by Radulescu *et al.* [50] appear consistent with the results presented here, however, a full comparison of conductivity measurements to the predictions of Radulescu *et al.* [50] would require shear step-up experiments, which is not done in the present work.

C. Fluctuations

Many shear-banded systems exhibit fluctuations in the position of the interface between the high and low shear rate bands. Such fluctuations can arise from inherent interface instability, from stick-slip at the wall and nucleation-melt cycles of the shear induced phase, or from bulk viscoelastic instability [20–24]. Indeed, the system under study has been found [13] to exhibit stress and velocity field fluctuations at applied shear rates above 4 s^{-1}. We note, as seen in Fig. 3(a), that the conductivity also exhibits temporal fluctuations at a level significantly greater than the measurement error (on the order of the size of a data symbol), and with a characteristic time on the order of a few seconds, again comparable with that found by López-González *et al.* [13].

IV. CONCLUSION

Our results show that the electrical conductivity measurement can be used to study shear banding in micellar solutions, and can be reliable complement in probing micellar orientation. Advantages of the conductivity method include the potential for applications in strongly scattering and opaque systems, and that in principle, the method can allow high temporal resolution. The main features of the flow curve are reproduced in the conductivity versus shear rate plots presented here. Significant factors that affect the slow growth of the anisotropy in the plateau region are wall slippage and short micellar lengths in the shear induced phase, with an estimated length to diameter ratio in the range of 5–15. The time resolved conductivity measurements in both geometries capture the transient behavior in shear banding, and is in good agreement with the results of other methods. The transient behavior of the conductivity shows that the overall anisotropy of the sample decreases as the steady state is approached, i.e., the micellar length/the degree of order decrease. The measurements reported here were obtained in two geometries (parallel to the velocity and parallel to the vorticity) with time resolution in the order of 0.5 s. In future work we hope to include the geometry parallel to the velocity gradient and achieve finer time resolution.

ACKNOWLEDGMENTS

Financial support from the Royal Society of New Zealand Marsden Fund and Centers of Research Excellence Fund are gratefully acknowledged.

[1] J.-F. Berret, in *Molecular Gels*, edited by R. G. Weiss, R. G. and P. Terech (Springer, Dordrecht, 2005) p. 235.
[2] M. E. Cates, T. C. B. McLeish, and O. Marrucci, EPL **21**, 451 (1993).
[3] N. A. Spenley, M. E. Cates, and T. C. B. McLeish, Phys. Rev. Lett. **71**, 939 (1993).
[4] N. A. Spenley, X. F. Yuan, and M. E. Cates, J. Phys. II **6**, 551 (1996).
[5] J. P. Decruppe, E. Cappelaere, and R. Cressely, J. Phys. II **7**, 257 (1997).
[6] A. F. Mendez-Sanchez, J. Perez-Gonzalez, L. deVargas, J. R. Castrejon-Pita, A. A. Castrejon-Pita, and G. Huelsz, J. Rheol. **47**, 1455 (2003).
[7] J. B. Salmon, A. Colin, S. Manneville, and F. Molino, Phys. Rev. Lett. **90**, 228303 (2003).
[8] R. W. Mair and P. T. Callaghan, EPL **36**, 719 (1996).
[9] J. Y. Lee, G. G. Fuller, N. E. Hudson, and X.-F. Yuan, J. Rheol. **49**, 537 (2005).
[10] Y. T. Hu and A. Lips, J. Rheol. **49**, 1001 (2005).
[11] L. R. Rossi, G. McKinley, and L. P. Cook, J. Non-Newtonian Fluid Mech. **136**, 79 (2006).
[12] M. R. López-González, W. M. Holmes, P. T. Callaghan, and P. J. Photinos, Phys. Rev. Lett. **93**, 268302 (2004).
[13] M. R. López-González, W. M. Holmes, and P. T. Callaghan, Soft Matter **2**, 855 (2006).
[14] S. Lerouge, M. Argentina, and J. P. Decruppe, Phys. Rev. Lett. **96**, 088301 (2006).
[15] S. Lerouge, M. A. Fardin, M. Argentina, G. Grégoire, and O.

Cardoso, Soft Matter **4**, 1808 (2008).
[16] M. A. Fardin, B. Lasne, O. Cardoso, G. Gregoire, M. Argentina, J. P. Decruppe, and S. Lerouge, Phys. Rev. Lett. **103**, 028302 (2009).
[17] S. Lerouge, J. P. Decruppe, and P. Olmsted, Langmuir **20**, 11355 (2004).
[18] E. Miller and J. P. Rothstein, J. Non-Newtonian Fluid Mech. **143**, 22 (2007).
[19] J.-F. Berret, Langmuir **13**, 2227 (1997).
[20] M. P. Lettinga and S. Manneville, Phys. Rev. Lett. **103**, 248302 (2009).
[21] S. M. Fielding and P. D. Olmsted, Phys. Rev. Lett. **92**, 084502 (2004).
[22] S. M. Fielding and P. D. Olmsted, Phys. Rev. Lett. **96**, 104502 (2006).
[23] S. M. Fielding, Phys. Rev. E **76**, 016311 (2007).
[24] S. M. Fielding, Soft Matter **3**, 1262 (2007).
[25] J. M. Adams, S. M. Fielding, and P. D. Olmsted, J. Non-Newtonian Fluid Mech. **151**, 101 (2008).
[26] S. Manneville, Rheol. Acta **47**, 301 (2008).
[27] P. T. Callaghan, Rheol. Acta **47**, 243 (2008).
[28] M. E. Cates and S. M. Fielding, Adv. Phys. **55**, 799 (2006).
[29] P. D. Olmsted, Rheol. Acta **47**, 283 (2008).
[30] E. Cappelaere, R. Cressely, R. Makhloufi, and J. P. Decruppe, Rheol. Acta **33**, 431 (1994).
[31] J. P. Decruppe, R. Cressely, R. Makhloufi, and E. Cappelaere, Colloid Polym. Sci. **273**, 346 (1995).
[32] H. Rehage and H. Hoffmann, Rheol. Acta **21**, 561 (1982).
[33] H. Rehage and H. Hoffmann, J. Chem. Phys. **92**, 4712 (1988).
[34] J.-F. Berret, D. Roux, and G. Porte, J. Phys. II **4**, 1261 (1994).
[35] J.-F. Berret, G. Porte, and J. P. Decruppe, Phys. Rev. E **55**, 1668 (1997).
[36] R. Oda, P. Panizza, M. Schmutz, and F. Lequeux, Langmuir **13**, 6407 (1997).
[37] R. Sanchez, J. Perez-Gonzalez, and L. de Vargas, J. Non-Newtonian Fluid Mech. **149**, 71 (2008).
[38] K. G. Gotz and K. Heckmann, J. Colloid Sci. **13**, 266 (1958).
[39] A. Nesrullajev, N. Kazanci, and T. Yildiz, Mater. Chem. Phys. **80**, 710 (2003).
[40] P. Photinos, S. Y. Xu, and A. Saupe, Phys. Rev. A **42**, 865 (1990).
[41] G. G. Fuller, *Optical Rheometry of Complex Fluids* (Oxford University Press, New York, 1995).
[42] B. A. Schubert, N. J. Wagner, E. W. Kaler, and S. R. Raghavan, Langmuir **20**, 3564 (2004).
[43] P. Photinos, in *Phase Transitions in Complex Fluids*, edited by P. Toledano and A. F. Neto (World Scientific Publishing, Singapore, 1998), p. 173.
[44] P. Photinos, G. Melnik, and A. Saupe, J. Chem. Phys. **84**, 6928 (1986).
[45] H. Fricke, J. Phys. Chem. **57**, 934 (1953).
[46] P. Photinos and A. Saupe, Mol. Cryst. Liq. Cryst. **98**, 91 (1983).
[47] J.-F. Berret, D. C. Roux, and P. Lindner, Eur. Phys. J. B **5**, 67 (1998).
[48] L. Onsager, Ann. N.Y. Acad. Sci. **51**, 627 (1949).
[49] W. M. Holmes, M. R. López-González, and P. T. Callaghan, EPL **66**, 132 (2004).
[50] O. Radulescu, P. D. Olmsted, J. P. Decruppe, S. Lerouge, J.-F. Berret, and G. Porte, EPL **62**, 230 (2003).